NDT&E International 139 (2023) 102918

Contents lists available at ScienceDirect

NDT and E International

journal homepage: www.elsevier.com/locate/ndteint

In-situ dynamic monitoring of phase transformation in steels using a multi-frequency electromagnetic sensor

L. Zhou [a,*], W. Jacobs [b], F. Wu [a], M. Jolfaei [a], C.L. Davis [a]

[a] WMG, University of Warwick, Coventry, CV4 7AL, United Kingdom
[b] Primetals Technologies Ltd, Christchurch, BH23 6EW, United Kingdom

ARTICLE INFO

Keywords:
Dynamic transformation measurement
Steel microstructure
EM sensors
Relative magnetic permeability
FE modelling

ABSTRACT

An industrial-scale electromagnetic (EM) sensor is employed to non-destructively and dynamically monitor the microstructural phase transformation for mild steel samples with different thicknesses (3 mm, 6 mm, and 10 mm), high carbon steel (0.76 wt% C) and 2.25Cr–1Mo steel plates. The continuous cooling process of these samples in ambient air (cooling rate of 0.99–7.53 °C/s) on a run-out table is examined. To determine the phase fractions based on the EM sensor signal and measured temperature, a finite element (FE) model for the EM sensor is utilised. The obtained phase fractions are further validated by conducting dilatometry measurements independently, confirming the accuracy of the transformation behaviour and phase fraction determination derived from the EM sensor readings.

1. Introduction

The production of modern high-performance structural steel grades requires tight control of the thermo-mechanical processing parameters to achieve the desired microstructure and mechanical properties. Hot rolling, followed by a dynamic cooling process on the run-out table, where significant phase transformation is achieved before the coiling of the strip, has a significant impact on the mechanical properties of the hot-rolled products. It is beneficial to be able to monitor the microstructure changes online dynamically and non-destructively. Non-destructive testing techniques, such as X-ray, ultrasonic and electromagnetic sensors, have been demonstrated for steel microstructure characterisation [1–15], among which electromagnetic (EM) sensors are good candidates for online microstructure measurement due to their advantages of being safe, non-contact, having a fast response time, relatively low cost and are not adversely affected by the measurement environment (dust or steam). EM sensors work by detecting magnetic permeability and electrical conductivity changes, which are sensitive to microstructure changes such as grain size, phase balance, and precipitates due to their influence magnetic permeability (dominant effect) and electrical conductivity (minor effect).

Multi-frequency low magnetic field EM sensors have been used in a lab environment to quantify the ferrite – pearlite phase balance in C–Mn steel [16,17] and ferrite - martensite phase balance in DP steel at room temperature [18]. The sensors are also being used to assess the microstructure status of power plant steel grades, considering changes in the martensitic structures due to thermal exposure [19,20]. In addition, low-field EM coil shaped sensors have been used to detect transformation in hot rod or strip samples during continuous heating and cooling in a laboratory setup [3,21–23], where, samples were stationary placed within the sensing coils during heating and cooling. In commercial applications, high magnetic field strength (>2 kA/m) EM sensors such as the IMPOC, HACOM and 3 MA system are used online in cold strip mills to directly correlate measured signals to the mechanical properties [24–26]. EMspec™ sensors have been installed at a hot strip mill to detect and monitor phase transformation via high-temperature in-situ measurements in the run out table [14]. The harsh environmental conditions in the run out table mean that the sensors are located at a relatively large lift-off distance to the hot steel strip and are cased in a cooled canister; this results in a low applied magnetic field at the target sample. The sensor uses the 'zero crossing frequency (ZCF)' measurement, as it is closely related to the relative permeability value of the steel and is less sensitive to variations in the lift-off than the inductance value [27]. The EMspec™ sensor signal has been shown to measure the transformed ferrite-phase fractions for a plain carbon steel grade on the run out table in a hot strip mill, with the measurement results agreeing well with predicted transformed fraction based on thermodynamic - metallurgical phase transformation mill models [28].

* Corresponding author.
E-mail address: lei.zhou@warwick.ac.uk (L. Zhou).

https://doi.org/10.1016/j.ndteint.2023.102918
Received 20 February 2023; Received in revised form 20 June 2023; Accepted 20 July 2023
Available online 22 July 2023

To interpret the EM signal it is necessary to predict the relative magnetic permeability from the microstructural parameters and then link the permeability to the sensor output. The effect of ferrite fraction (in ferrite–pearlite and ferrite-austenite steels with uniform second phase distribution) on the relative permeability at room and elevated temperature has been determined using a finite element (FE) microstructure–magnetic property model using COMSOL Multiphysics [16,29]. In addition, a 3D FE EM sensor model has been developed, allowing the EMspec™ sensor output (ZCF) to be related to the magnetic relative permeability and electrical resistivity of the steel [30]. This paper uses the FE microstructure–magnetic property model and the FE EM sensor model to demonstrate the dynamic measurement of transformation for a range of structural steel grades using the EMspec™ sensor on a furnace and run-out table (ROT).

2. Materials and methods

A range of structural steel grades, including mild steel, high carbon steel, and 2.25Cr–1Mo steel were used in this study. The dimensions and chemical compositions for the samples are shown in Table 1.

Metallographic samples were taken in the transverse direction, polished to an OPS finish and etched in 2% nital. The samples were imaged using a Zeiss Akioskop-2 optical microscope equipped with Axiovision 4.6.3 image capture software.

A DIL805A/D dilatometer was used for the measurement of phase transformation for all the samples. Samples of 5 mm × 10 mm × thickness was heated to 980 °C in 5 min and held for 5 min. The cooling rate was programmed to reproduce the cooling trajectory measured for the 500 × 500 mm samples on the ROT. The transformation fraction was calculated using the Lever rule calculation described in [31].

The EMspec™ sensor used in this study was provided by Primetals Technologies Ltd. The sensor consists of an H-shaped non-conducting ferrite core with an exciting coil and two sensing coils (one dummy and one active). The sensor is embedded in a ferritic stainless steel canister which is used to shield the sensor signal from the surrounding environment (such as run out table rollers) and is water-cooled during the tests to protect the sensor. The canister is installed between the rollers of the run-out table (ROT).

The sensor head is set at a 40 mm lift off from the sample. Images of the experimental setup are shown in Fig. 1. The EMspec™ sensor works by generating an applied field **H,** simultaneously at 8 frequencies at 375, 750, 1500, 3000, 6000, 12,000, 24,000, and 48000 Hz, using the exciting coil. The depth to which a magnetic field can penetrate follows the skin effect rule. Lower magnetic relative permeability, electrical conductivity, and exciting frequencies result in greater penetration depth. The studies in the paper have a very slow heating and cooling rate for the steel samples. Therefore a uniform temperature profile through the sample thickness has been considered. The applied magnetic field **H** to the steel samples are relative low (<150A/m measured in the FE model), which corresponds to the Rayleigh region of the initial magnetisation curve [32]. The change in flux density **B** in the sample results in inductance in the active sensing coil, while the dummy coil inductance is dominated by the stainless steel canister. As the EMspec™ sensor output, the zero-crossing frequency (ZCF) values are calculated for each 'time stamp' using the measured phase angles at all eight frequencies. ZCF is defined as the frequency at which the phase angle between the real and imaginary parts of the inductance (sum of dummy and active coil inductance) equals −90°. The ZCF is proven to be closely related to the dot product of relative permeability and electrical resistivity of the sample and has the benefit of being relatively less sensitive to the changes in the lift off values (distance between the sample and the sensor head) [27].

The furnace and ROT system is designed to be an automated system to simulate the industrial strip sample cooling, albeit without prior hot deformation. Powered rollers are installed both at the ROT as well as inside of the furnace to allow a smooth transition of the steel sample to and from the furnace and then over the sensor when cooling. The ROT system is capable of applying air, forced air and controlled water cooling. In this study, all samples were pre-heated to 980 °C, held for 5 min and then moved onto the ROT for transformation monitoring during air cooling. K-type thermocouples with a fiberglass sheath were attached to the top surface of the samples and are used to monitor the temperature of the sample.

The EM sensor output ZCF values were converted into transformation fractions using the combination of the FE microstructure–magnetic property model and the FE EM sensor model. The details of the models are described in Refs. [29,30], respectively. In the microstructure–magnetic property model, simulated 3D dual-phase (austenite and ferrite) microstructures with a second phase fraction of 0–100% in 5% steps were generated by an advanced Voronoi-based algorithm [33]. The microstructural phases were considered as constituents with different relative permeability values, which were determined experimentally for austenite + pearlite (for the high carbon steel) and austenite + ferrite (for the mild steel) with temperature [29]. For Cr–Mo steel, austenite + bainite phase balance was considered. The low field relative permeability value of bainite of 88 was measured for the Cr–Mo steel. A parallel trend of how much permeability change with respect to temperature was assumed for bainite in compare to that of the pearlite. The assumption was based on that both bainite and pearlite microstructures have a large number of domain pinning sites finely spaced carbides. The austenite phase is considered paramagnetic; hence relative permeability of 1 is used across the temperature range used in this study. The effective relative permeability of the austenite–second phase mixtures were then calculated by the modelled average flux density **B** and the applied field **H** in the sample. The 3D FE EM sensor model has the detailed sensor and sample geometry for the EMspec™ system and 500 × 500 mm samples and was used to calculate the effective relative magnetic permeability values from the microstructure–magnetic property model and electrical resistivity values with temperature from the literature [34] to calculate the sensor output. The modelled relative permeability and hence ZCF values for different combinations of phase type, phase fraction, and temperature are used, as a look up table, to calculate the transformation fraction from the experimentally measured ZCF values.

3. Results and discussion

3.1. Mild steel plates of different thickness

The microstructure of the 3 mm, 6 mm and 10 mm mild steel samples in the as-received condition and after reheating and cooling on the ROT are shown in Figs. 2 and 3, respectively. The as-received samples show a

Table 1
Dimensions and chemical compositions of steels in wt%.

Sample name	Dimensions (mm)	C	Si	Mn	P	S	Cr	Mo	Ni
Mild-3mm	500 × 500 × 3	0.16	0.01	0.81	0.007	0.003	0.018	0.0025	0.007
Mild-6mm	500 × 500 × 6	0.17	0.035	0.83	0.015	0.009	0.033	0.0018	0.013
Mild-10mm	500 × 500 × 10	0.18	0.009	0.87	0.015	0.012	0.015	0.001	0.003
High Carbon-3mm	415 × 460 × 3	0.76	0.197	0.72	0.007	0.0005	0.166	0.016	0.067
Cr–Mo-3mm	500 × 500 × 3	0.11	0.29	0.58	0.013	0.002	2.12	0.94	0.06

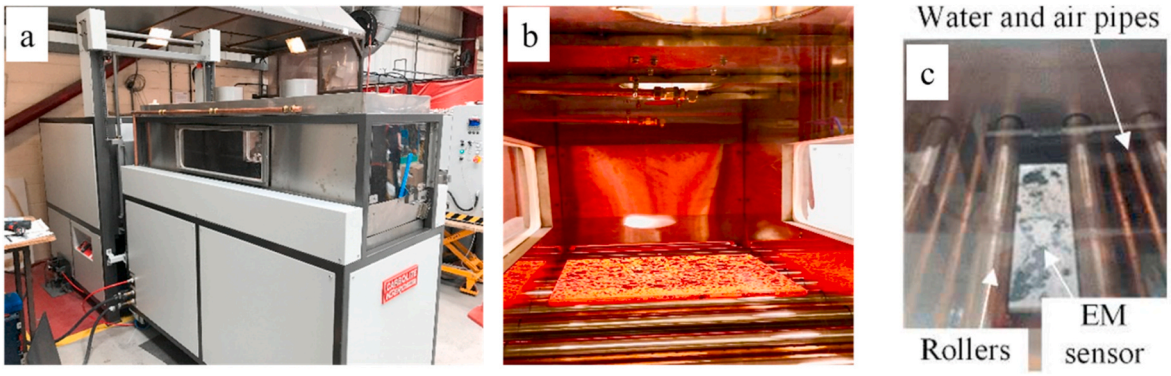

Fig. 1. a) Images of the furnace and run-out table system, b) image of a hot steel plate placed on the runout table above the sensor location, and c) the EMspec™ sensor in its protective housing installed between the rollers on the runout table.

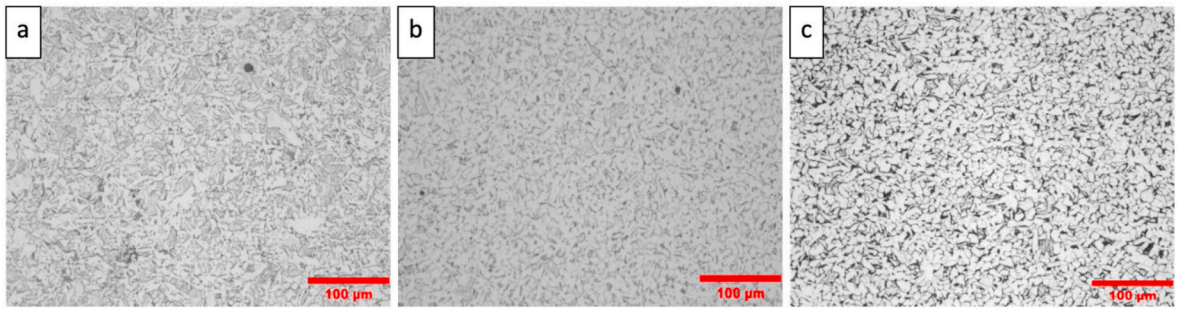

Fig. 2. Optical micrographs of the a) 3 mm, b) 6 mm and c) 10 mm mild steel samples in as-received condition.

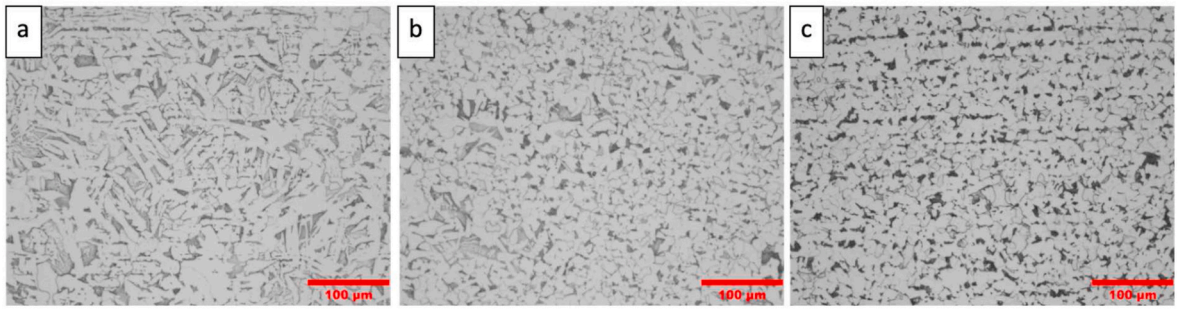

Fig. 3. Optical micrographs of the a) 3 mm, b) 6 mm and c) 10 mm mild steel samples after reheating and cooling.

ferrite matrix with randomly distributed pearlite and bainite phase. After the heat treatment, the microstructure has coarsened with an increase in ferrite grain size, caused by the relatively high austenising temperature (980 °C) and the slow cooling rate. The ferrite fraction measured for the 6 and 10 mm sample before and after the heat treatment is 80% ± 2%. However, the measured ferrite fraction for the 3 mm sample before and after the heat treatment is 70% ± 5%. This is because the 3 mm sample has higher bainite to pearlite ratio than the 6 mm and 10 mm sample after the heat treatment. As the carbide content in bainite is less than in pearlite, formation of the bainite instead of pearlite results in higher volume fraction of second phase. The relative permeability of bainite is expected to be very similar to that of pearlite [35]. It should be noted that the relative permeability value, hence the EM sensor signal, can be affected by factors such as phase balance, ferrite grain size, pearlite interlamellar spacing, texture, stress and temperature. In this work, all samples are stress-free, and the variation in phase balance and temperature has the dominant effect on the relative permeability values and is considered in this work [16].

The measured cooling trajectories for the 3 mm, 6 mm and 10 mm mild steel strip samples during sensor measurements are shown in Fig. 4. As expected, the cooling rate decreases with increased sample thickness. Evidence of latent heating during transformation was shown in all samples. The first change in cooling temperature gradient due to latent heating happens at around 740 °C, which is consistent with the start of the austenite to ferrite transformation. A second change in cooling temperature gradient due to latent heating occurs at around 640 °C, which is believed to be due to the austenite to pearlite transformation. When compared to the thinner sample, the thicker sample shows a more noticeable latent heat effect. This is because the thicker sample has a larger volume, which produces more heat that takes longer to spread to the surface. The thermal conductivity of the material limits this diffusion process. The average cooling rates for the 3 mm, 6 mm and 10 mm mild steel samples between 980 °C and 500 °C, the temperature range where transformation happened, were calculated to be 3.04, 1.57 and 0.99 °C/s respectively.

The EMSpec™ sensor output (ZCF) versus temperature for the 3 mm, 6 mm and 10 mm mild steel sample cooling from 980 °C is shown in Fig. 5. It can be seen that the same sample grade mild steel sample with

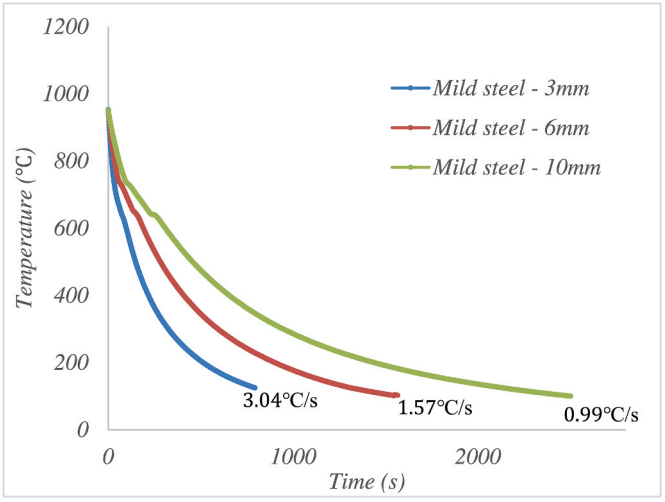

Fig. 4. The measured cooling trajectories for the 3 mm, 6 mm and 10 mm mild steel during sensor measurements. Cooling rates between 980 °C and 500 °C are shown for each sample.

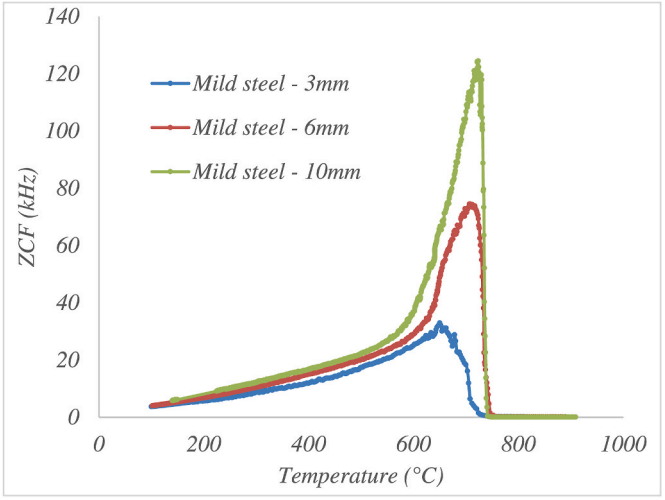

Fig. 5. ZCF versus temperature for 3 mm, 6 mm and 10 mm mild steel during cooling.

different thicknesses can be distinguished from the sensor output. At the highest temperature, around 980 °C, the ZCF values are very low, as the steel samples are paramagnetic above the Curie point. In addition, the microstructure phase of all three samples should be 100% austenite, which would also be paramagnetic at this temperature. As the steel samples cool, the ZCF for the 10 mm sample begins to increase at approximately 740 °C and peaks at 122 kHz at around 720 °C. The temperature is below the Curie temperature for this steel (approximately 760 °C). Hence the increase in ZCF is believed to be due to the austenite to ferrite transformation. ZCF can be affected by both relative magnetic permeability and the electrical resistivity of the sample. At 720 °C the electrical resistivity changes from 1.02 μΩm for austenite to 0.93 μΩm for ferrite phase, which will have a small change on the ZCF values. In comparison, the relative magnetic permeability changes from 1 for austenite to 6980 for ferrite at this temperature, which clearly dominates the signal changes. After the peak, the ZCF decreases with the temperature, which is associated with a decrease in relative permeability and electrical resistivity of the sample as the temperature decreases (i.e. temperature effect) [29]. For the 6 mm sample, the ZCF value increases sharply at 743 °C until reaching a peak at 73 kHz at around 705 °C. This is consistent with the austenite to ferrite transformation. After the peak, the ZCF begins to decrease with temperature until approximately 650 °C, where the gradient becomes steeper. In the temperature range of 705–650 °C, the 6 mm and 10 mm sample are still likely to be undergoing transformation, including from the remaining austenite phase to pearlite. The increase in relative permeability due to the remaining austenite (approx. 20%) to pearlite transformation is not as significant as the initial ferrite formation (as pearlite has a lower permeability than ferrite (~500 compared to ~7000 at this temperature range [29]) and therefore effectively masked by the decrease in relative permeability due to the temperature effect. The combined effect of transformation and decrease in temperature leads to a less steep decrease in ZCF between 710 °C and 650 °C. After 650 °C, the sample should have completed phase transformation and the ZCF continues to decrease with temperature due to the temperature effect. The 3 mm thick sample has the fastest cooling rate of the three thicknesses, which results in the transformation starting at a lower temperature than for the 10 mm and 6 mm mild steel. This is shown by the ZCF starting to increase at the lowest temperature (727 °C) of the three thicknesses and peaks at 31 kHz at 645 °C. The lower ZCF peak value is caused by the fact that the transformation starts at a lower temperature due to the faster cooling rate and permeability being strongly temperature dependent.

The EM sensor measured ferrite transformation fraction was predicted from the dynamic EM sensor output (ZCF values) for the 3 mm, 6 mm, and 10 mm mild steel samples, using the combination of the FE microstructure–magnetic property model and the FE EM sensor model.

The measured ferrite transformation fraction from the EM sensor, for the three thickness samples, and the dilatometry test data, determined for the three cooling rates relevant for the three thickness samples, are shown in Fig. 6. It can be seen that the EM sensor predicts a similar starting transformation temperature for the 6 mm and 10 mm samples in comparison with the dilatometry results. However, the EM sensor predicted a earlier finish transformation temperature than dilatometry. As discussed earlier, the relative magnetic permeability change is dominated by the austenite to ferrite transformation, whereas the dilatometry also shows the final austenite to pearlite transformation, which happened at a lower temperature, hence than change in gradient. For the 3 mm sample, the EM sensor predicts an earlier starting and finishing transformation than the dilatometry results. This is caused by the difference in the transformation behaviour during the ROT and the dilatometry test. The microstructure of the 3 mm sample shows ferrite and pearlite phases, whereas the microstructure of the sample after the ROT test shows ferrite and bainite phases. The continuous cooling transformation (CCT) diagram of the 3 mm mild steel sample predicted using

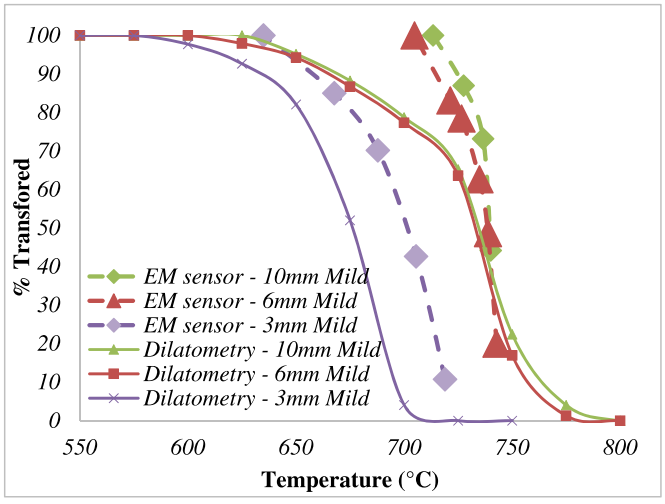

Fig. 6. EM sensor and dilatometry measured transformed fraction versus temperature for 3 mm, 6 mm and 10 mm mild steel samples.

JMatPro with an assumed austenite grain size of 20 μm is shown in Fig. 7. It can be seen that the cooling rate of around 3 °C for the 3 mm mild steel sample is very close to the nose of the bainite transformation. This means that a slight variation in the cooling rate between the ROT and dilatometry tests can cause significant differences in transformation behaviour and hence the microstructural phase formation.

3.2. High carbon steel

The microstructure of the high carbon steel samples in the as-received condition and after reheating and cooling on the ROT is fully pearlitic. The measured cooling trajectories for the 3 mm high carbon and the 3 mm mild steel during sensor measurements are shown in Fig. 8. The average cooling rates for the high carbon steel and the mild steel samples between 980 °C and 500 °C were calculated to be 7.5 and 3.04 °C/s, respectively. Significant latent heating occurs after initial cooling down to 615 °C for the high carbon steel due to the transformation to 100% pearlite. The difference in cooling rate for the same thickness samples is due to the difference in oxidation between the steels, with more oxide being formed on the 3 mm mild steel than on the high carbon steel (post-test observation).

The EMspec™ sensor output (ZCF) versus temperature for the 3 mm high carbon and the 3 mm mild steel sample cooling from 800 °C is shown in Fig. 9. The ZCF curve of the high-carbon steel is affected by latent heat. It can be seen that at around 630 °C, there is an increase in temperature as the ZCF increases. The mild steel has a higher ZCF peak value than the high carbon steel, as the mild steel transforms at a higher temperature than the high carbon steel, which is expected from the iron-carbon phase diagram. The difference in the ZCF values at the same temperature during cooling is due to the microstructure difference. The phase transformation in mild steel is mainly austenite to ferrite, whereas in high-carbon steel, austenite to pearlite transformation dominates. The ferrite phase has a higher relative permeability than pearlite. Therefore the ZCF value of mild steel remains higher than high carbon steel after the peak, and it is expected that the ZCF values would not come together even at room temperature. ZCF curves clearly distinguish the steel sample with different carbon content from the EMSpec™ sensor.

The pearlite transformation fraction results predicted by the EM sensor output and measured by dilatometry for the high carbon steel samples for the same cooling rate are shown in Fig. 10. It can be seen that the EM sensor predictions agree well with the dilatometry results. The transformation from austenite to pearlite occurs at a lower temperature (around 630 °C) than the austenite to ferrite transformation in the 3 mm mild steel (around 720 °C).

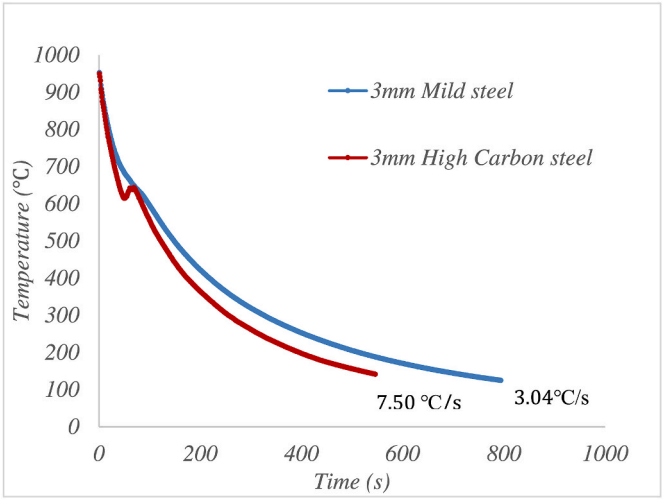

Fig. 8. The measured cooling trajectories for the 3 mm mild steel and high carbon steel samples during sensor measurements. Cooling rates between 980 °C and 500 °C are shown for each sample.

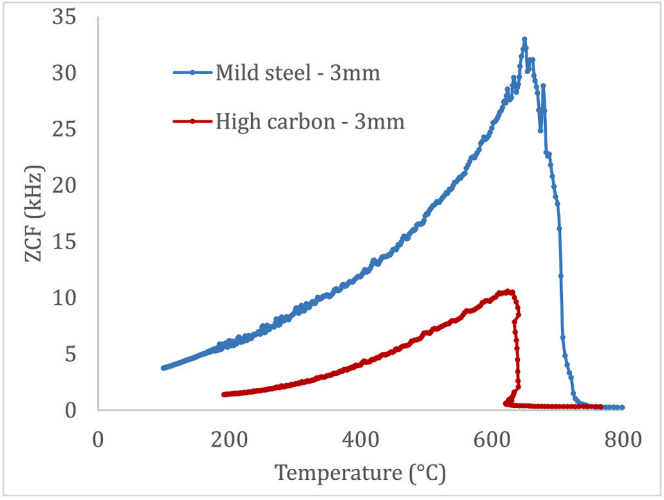

Fig. 9. ZCF versus temperature for the 3 mm high carbon steel and the 3 mm mild steel during cooling.

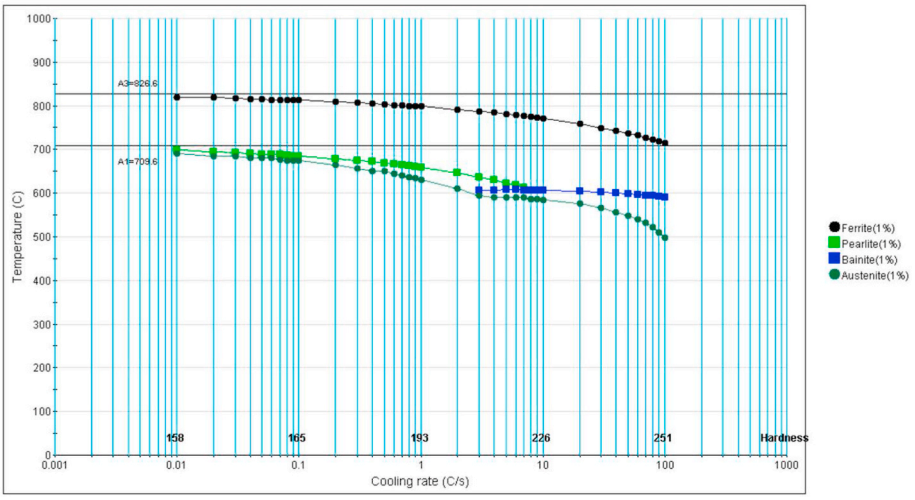

Fig. 7. Continuous cooling diagram for the 3 mm mild steel sample predicted using JMatPro software.

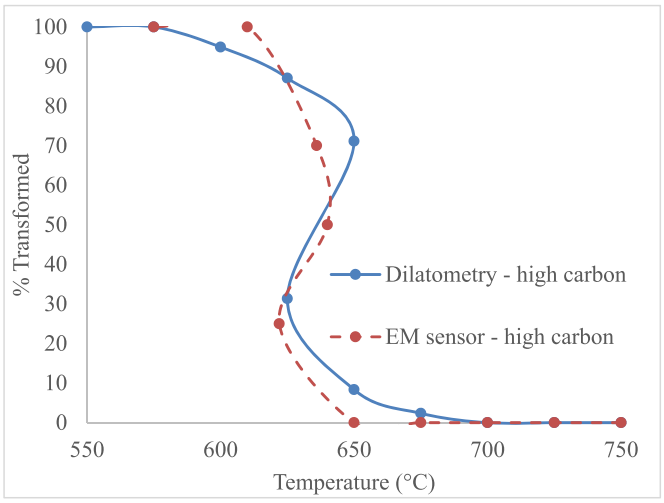

Fig. 10. EM sensor and dilatometry measured transformed fraction versus temperature for high carbon steel samples.

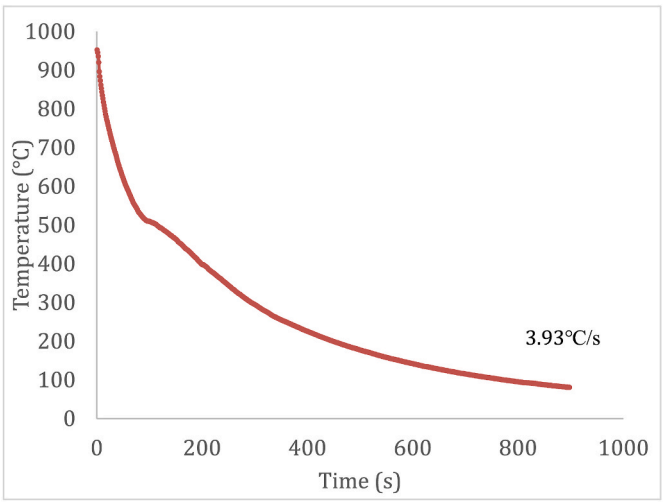

Fig. 12. The measured cooling trajectories for the Cr–Mo steel during sensor measurements. Cooling rates between 980 °C and 500 °C is shown.

3.3. Cr–Mo steel

The microstructure of the Cr–Mo steel samples in the as received condition and after reheating and cooling on the ROT are shown in Fig. 11. A fully bainitic microstructure can be observed for both samples before and after the heat treatment. The morphology of the bainitic microstructure changes slightly after the heat treatment. However, the change in relative magnetic permeability due to the different morphology of the bainitic structure is expected to be very small in comparison with the changes due to transformation [35].

The measured cooling trajectories for the Cr–Mo steel during sensor measurements are shown in Fig. 12. The average cooling rates for the Cr–Mo sample between 980 °C and 500 °C, is 3.93 °C/s. The cooling rate is slight higher than the 3 mm mild steel sample (3.04 °C/s) as there is less oxidation of the sample which can affect the cooling. The At around 500 °C, a change in cooling rate is seen due to the latent heating effect due to the transformation from austenite to bainite.

The EMspec™ sensor output (ZCF) versus temperature for the Cr–Mo steel sample cooling from 550 °C is shown in Fig. 13. The alloying elements of Cr and Mo significantly increase the hardenability of the steel; hence the austenite to bainite transformation is expected to happen at temperatures that are significantly lower than the Curie point of the steel. Above 520 °C, the ZCF values are very low, as the steel is 100% austenite, which is paramagnetic. As the steel samples cool, the ZCF begins to increase at approximately 500 °C and peaks at 5.5 kHz at around 403 °C. After the peak, the ZCF decreases with the temperature, which is associated with a decrease in relative permeability and electrical resistivity of the sample as the temperature decreases (i.e. temperature effect). The bainite transformation fraction results predicted by

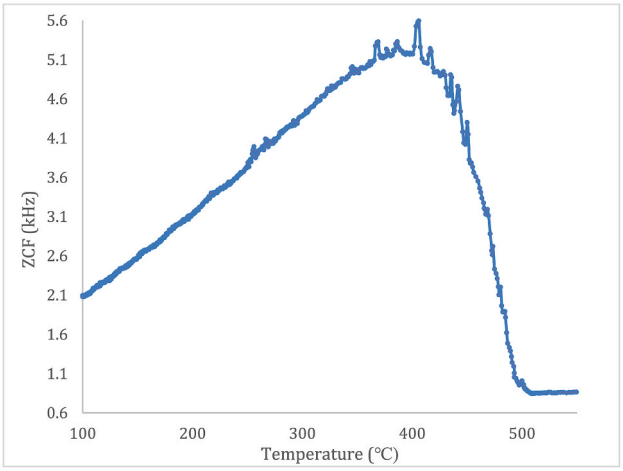

Fig. 13. ZCF versus temperature for the Cr–Mo steel during sensor measurements.

ZCF and measured by dilatometry for the Cr–Mo steel samples are shown in Fig. 14. It can be seen that the EM sensor predictions agree well with the dilatometry results.

Typically, dilatometry measurements, which rely on dimensional changes, are widely regarded as the most accurate method for measuring phase transformations. However, these measurements necessitate machining the sample into a small size and assuming a uniform

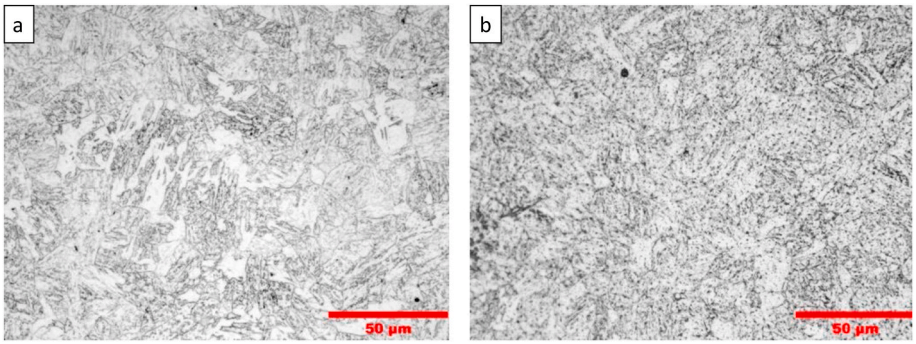

Fig. 11. Optical micrographs of the Cr–Mo steel samples in a) as-received condition and b) after the heat treatment.

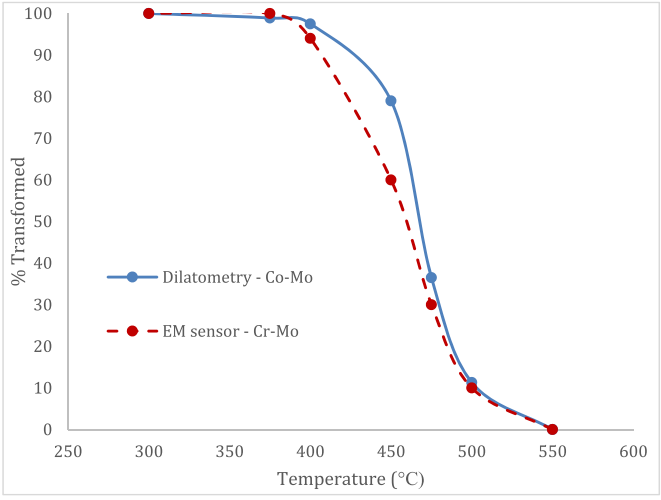

Fig. 14. EM sensor and dilatometry measured transformed fraction versus temperature for the Cr–Mo steel sample.

temperature and cooling profile throughout the sample. In contrast, the electromagnetic (EM) sensor can measure a significantly larger area, approximately 400 mm^2, making it more suitable for in-situ and dynamic monitoring of steel strips or plates during processing.

4. Conclusion

In this study, a recently developed industrial electromagnetic sensor (EMspec™) has been used to dynamically monitor the phase transformation behaviour of C–Mn and Cr–Mo steel plates during continuous cooling at a laboratory run-out table. The sensor signal (zero crossing frequency) has been converted into a phase transformed fraction using a previously developed finite element microstructure–magnetic property model and the electromagnetic sensor model. The transformation fraction measured by the sensor are in good agreement with independently measured transformation fraction using dilatometry. It is shown that the sensor can monitor phase transformation dynamically and that the differences in transformation fraction and transformation temperature (due to different steel composition or different cooling rates, due to different plate thickness) can be observed.

Author statement

Lei Zhou: Conceptualization; Data curation; Formal analysis; Investigation; Methodology; Project administration; Resources; Software; Validation; Visualization; Roles/Writing - original draft; Writing - review & editing. W. Jacobs: Data curation, Investigation. F. Wu, M. Jolfaei: Methodology, Data Curation, Claire Davis: Writing - review & editing; Supervision; Funding acquisition; Project administration.

Declaration of competing interest

The authors declare that they have no known competing financial interests or personal relationships that could have appeared to influence the work reported in this paper.

Data availability

Data will be made available on request.

Acknowledgements

The research leading to these results has received funding from EPSRC and Primetals Technologies Ltd via an ICASE studentship, EPSRC project RIME (EP/P027210/01), and the EPSRC SUSTAIN Manufacturing Hub (EP/S018107/1).

References

[1] Kopineck H-J, Löffel R, Otten H-B. Industrial on-line texture determination in rolled steel strips. J Nondestr Eval 1993;12:13–9. https://doi.org/10.1007/BF00565904.
[2] Hutchinson B, Moss B, Smith A, Astill A, Scruby C, Engberg G, Bjorklund J. Online characterisation of steel structures in hot stripmill using laser ultrasonic measurements. Ironmak Steelmak 2002;29:77.
[3] Papaelias MP, Strangwood M, Peyton AJ, Davis CL. Measurement and modeling of the electromagnetic response to phase transformation in steels. Metall Mater Trans 2004;35:965–72. https://doi.org/10.1007/s11661-004-1000-0.
[4] Biezma MV, Martin U, Linhardt P, Ress J, Rodríguez C, Bastidas DM. Non-destructive techniques for the detection of sigma phase in duplex stainless steel: a comprehensive review. Eng Fail Anal 2021;122:105227. https://doi.org/10.1016/J.ENGFAILANAL.2021.105227.
[5] Sheng H, Wang P, Tang C, Shi Y, Zheng Y. Microstructure and mechanical properties evaluation of automotive plate steel based on micromagnetic NDT technologies. Measurement 2022;199:111459. https://doi.org/10.1016/J.MEASUREMENT.2022.111459.
[6] Zelin M. Microstructure evolution in pearlitic steels during wire drawing. Acta Mater 2002;50:4431–47. https://doi.org/10.1016/S1359-6454(02)00281-1.
[7] Pereira HB, Echeverri EAA, Centeno DMA, de Souza S da S, Bauri LF, Manfrinato MD, Masoumi M, Alves LHD, Goldenstein H. Effect of pearlitic and bainitic initial microstructure on cementite spheroidization in rail steels. J Mater Res Technol 2023;23:1903–18. https://doi.org/10.1016/J.JMRT.2023.01.087.
[8] Karami Nezhad K, Kahrobaee S, Ahadi Akhlaghi I. Application of magnetic hysteresis loop method to determine prior austenite grain size in plain carbon steels. J Magn Magn Mater 2019;477:275–82. https://doi.org/10.1016/j.jmmm.2019.01.074.
[9] Dubois M, Moreau A, Militzer M, Bussière JF. Laser-ultrasonic monitoring of phase transformations in steels. Scripta Mater 1998;39:735–41. https://doi.org/10.1016/S1359-6462(98)00179-1.
[10] Malmström M, Jansson A, Hutchinson B. Application of laser-ultrasonics for evaluating textures and ani- sotropy. 2022. p. 1–13.
[11] Scruby CB, Smith RL, Moss BC. Microstructural monitoring by laser-ultrasonic attenuation and forward scattering. NDT E Int 1986;19:307–13. https://doi.org/10.1016/0308-9126(86)90001-5.
[12] Tolchard JR, Sømme A, Solberg JK, Solheim KG. On the measurement of austenite in supermartensitic stainless steel by X-ray diffraction. Mater Char 2015;99:238–42. https://doi.org/10.1016/j.matchar.2014.12.005.
[13] Bénéteau A, Aeby-Gautier E, Geandier G, Weisbecker P, Redjaïmia A, Appolaire B. Tempering of a martensitic stainless steel: Investigation by in situ synchrotron X-ray diffraction. Acta Mater 2014;81:30–40. https://doi.org/10.1016/j.actamat.2014.07.050.
[14] Sommers U, Klinkenberg C, Daube T, Brühl F, Sasse C, Gmbh SMS, Ionescu C, Sasse C. X-CAP -Closed-loop control of the AHSS annealing process via X-ray phase fraction measurement Contact data X-CAP – closed-loop control of the AHSS annealing process via X-ray phase fraction measurement. 2019.
[15] Fu B, Yang WY, Wang YD, Li LF, Sun ZQ, Ren Y. Micromechanical behavior of TRIP-assisted multiphase steels studied with in situ high-energy X-ray diffraction. Acta Mater 2014;76:342–54. https://doi.org/10.1016/j.actamat.2014.05.029.
[16] Zhou L, Liu J, Hao XJ, Strangwood M, Peyton AJ, Davis CL. Quantification of the phase fraction in steel using an electromagnetic sensor. NDT E Int 2014;67:31–5. https://doi.org/10.1016/j.ndteint.2014.06.007.
[17] Thompson SM, Tanner BK. The magnetic properties of pearlitic steels as a function of carbon content. J Magn Magn Mater 1993;123:283–98. https://doi.org/10.1016/0304-8853(93)90454-A.
[18] Jolfaei M, Zhou L, Davis CL, Loop O, Sensors D. Consideration of magnetic measurements for characterisation of ferrite – martensite commercial DP steel and basis for opti- misation of the operating. Magnetic Field for Open Loop De- ployable Sensors 2021;11(490):1–14.
[19] Karimian N, Wilson JW, Peyton AJ, Yin W, Liu J, Davis CL. Differential permeability behaviour of P9 and T22 power station Steels. J Magn Magn Mater 2014;352:81–90. https://doi.org/10.1016/j.jmmm.2013.09.059.
[20] Liu J, Hao XJ, Zhou L, Strangwood M, Davis CL, Peyton AJ. Measurement of microstructure changes in 9Cr–1Mo and 2.25Cr–1Mo steels using an electromagnetic sensor. Scripta Mater 2012;66:367–70. https://doi.org/10.1016/j.scriptamat.2011.11.032.
[21] Bruchwald O, Frąckowiak W, Reimche W, Frąckowiak W, Reimche W. Non-destructive in situ monitoring of the microstructural development in high performance steel components during heat treatment. 2015.
[22] Kuz'ko EI, Belomyttsev MYu, Belov VA, Kuz'ko EI, Belomyttsev MYu, Belov VA. A study of phase transformations in high-chromium ferritic-martensitic steels by magnetometry. MSHT 2018;60:259–65. https://doi.org/10.1007/S11041-018-0270-X.
[23] Leonhardt A, Wendler F, Wertheim R, Kräusel V, Kanoun O. Induction coil as sensor for contactless, continuous in-process determination of steel microstructure by means of Magnetic Induction Spectroscopy (MIS). CIRP J Manuf Sci Technol 2021;33:240–6. https://doi.org/10.1016/j.cirpj.2021.03.011.
[24] Skarlatos A. Modelling the IMPOC response for different steel strips. WCNDT; 2016.

[25] Kroos J, Stolzenberg M, Evertz T, Westkämper G. Combined measuring system for an improved non-destructive determination of the mechanical/technological material properties of steel sheet. Publications Office of the European Union; 2005.
[26] Gabi Y, Kedous-Lebouc A, Meunier G, Wolter B, Geoffroy O, Meilland P, Labie P, Guérin C, Martins O. Assessment of 3MA technique potentiality for nondestructive evaluation of dual-phase steels using 2-D nonlinear FEM and taking hysteretic behavior into account. In: Proc. 19th conf. Comput. Electromagn.Fields; 2013.
[27] Yin W, Peyton AJ, Strangwood M, Davis CL. Exploring the relationship between ferrite fraction and morphology and the electromagnetic properties of steel. J Mater Sci 2007;42:6854–61. https://doi.org/10.1007/s10853-006-1327-6.
[28] Yang H, Van den Berg FD, Luinenburg A, Bos C, Kuiper G, Mosk J, Hunt P, Dolby M, Flicos M, Peyton A, Davis C. In-line quantitative measurement of transformed phase fraction by EM sensors duing ControLled cooling on the run-out table of a hot strip mill. In: 19th world conference on non-destructive testing; 2016. p. 1–8.
[29] Zhou L, Hall R, Davis CL. Measured and modelled low field relative permeability for dual phase steels at high temperature. J Magn Magn Mater 2019;475:38–43. https://doi.org/10.1016/j.jmmm.2018.11.096.
[30] Shen J, Zhou L, Jacobs W, Hunt P, Davis C. Real-time in-line steel microstructure control through magnetic properties using an EM sensor. J Magn Magn Mater 2019;490:165504. https://doi.org/10.1016/j.jmmm.2019.165504.
[31] Quidort D, Brechet YJM. A model of isothermal and non isothermal transformation. ISIJ Int 2002;42:1010–7.
[32] Bozorth RM. Ferromagnetism. New York: Van Nostrand; 1965.
[33] Zhou L, Davis CL, Kok PJJ, van den Berg F, van den Berg F. Magnetic NDT for steel microstructure characterisation – modelling the effect of second phase distribution on magnetic relative permeabilty. WCNDT; 2016. p. 1–8.
[34] ASM handbook, volume 1: properties and selection: irons, steels, and high-performance alloys. ASM International; 2017.
[35] Zhou L. Non-destructive characterisation of steel microstructures using electromagnetic sensors. 2015.